Journal of Optics A: Pure and Applied Optics

Compensation of longitudinal dispersion for the GI2T-REGAIN* optical interferometer

To cite this article: Nathalie Thureau 2001 *J. Opt. A: Pure Appl. Opt.* **3** 440

View the article online for updates and enhancements.

Related content

- The Navy Prototype Optical Interferometer
- Vision: A Six-telescope Fiber-fed Visible Light Beam Combiner for the Navy Precision Optical Interferometer
- Progress in ground-based optical telescopes

Recent citations

- D. Mourard *et al*

This content was downloaded from IP address 193.54.110.59 on 11/11/2020 at 14:49

INSTITUTE OF PHYSICS PUBLISHING JOURNAL OF OPTICS A: PURE AND APPLIED OPTICS

J. Opt. A: Pure Appl. Opt. **3** (2001) 440–445 PII: S1464-4258(01)22958-4

Compensation of longitudinal dispersion for the GI2T-REGAIN* optical interferometer

Nathalie Thureau[1]

Observatoire de la Côte d'Azur (O.C.A), 2130 route de l'Observatoire, F-06460 Caussols, France

E-mail: thureau@mrao.cam.ac.uk

Received 16 March 2001, in final form 9 August 2001
Published 12 September 2001
Online at stacks.iop.org/JOptA/3/440

Abstract
We describe an optical system which corrects the effects of longitudinal dispersion for the GI2T-REGAIN optical interferometer. This system, now complete, should dramatically improve the observing efficiency of the dual-mode GI2T focal spectrograph. We first present the results of an analytical study and numerical simulations to optimize both the classical dispersed multi-speckle and new full-size filtered speckle interferograms from GI2T. This will be the first time a unique dispersion-compensating system attains very low visibility losses simultaneously in the narrow and large spectral bandwidth operating modes specified on GI2T. According to our concept the theoretical losses remain well below the 1% overall tolerance budget defined for the GI2T-REGAIN project. The importance of such a result is well understood since, within the same observing conditions, the use of the full-size interferograms should represent a signal-to-noise ratio 5× that of the classical operating dispersed fringe mode of GI2T.

Keywords: Longitudinal dispersion, stellar optical interferometry, multi-speckle mode

1. Introduction

Ground long baseline optical arrays need delay lines to equalize their optical path lengths. With delay lines, one attempts to balance a vacuum path difference that arises in space. The best compensation for that optical path difference (OPD) is obtained with the delay line operating in vacuum. An alternative method consists in performing the compensation in air. The residual OPD caused by the air, which is a dispersive medium, can be corrected by introducing glass plates in each interferometric arm. Among the existing interferometric arrays, both solutions are equally utilized. MarkIII, NPOI (Navy Prototype Optical Interferometer) and IOTA (Infrared Optical Telescope Array) arrays include vacuum pipes to feed the focal instrumentation. The optical path compensation is then ensured by delay lines that are located in large vacuum tanks. The glass option has been chosen for dispersion correction within the SUSI (Sydney University Stellar Interferometer, [2, 3]) and CHARA (Center for High Angular Resolution Astronomy, [15]) arrays. Since the expected dispersion effect at 2.2 μm can be neglected, the VLTI (Very Large Telescope Interferometer) has no dispersion correction system implemented. Glass correctors will be nevertheless implemented for future extension of the instrument to visible wavelengths [9]. COAST (Cambridge Optical Aperture Synthesis Telescope, [4]) does not compensate for atmospheric dispersion since the interferometer uses a channelled spectrum configuration, which allows one to avoid the problem. The question of longitudinal dispersion for the previous configuration of the GI2T interferometer was addressed by I Tallon-Bosc during her PhD Thesis [14]. The work presented in this paper, encouraged by the former results, integrates the features and complexity of the new GI2T-REGAIN instrumentation.

* GI2T: Grand Interféromètre à 2 Télescopes, REGAIN: Recombinateur du Grand Interféromètre.

[1] Now at Astrophysics Group, Cavendish Laboratory, Madingley Road, Cambridge CB3 OHE, UK.

© 2001 IOP Publishing Ltd Printed in the UK

Table 1. Summary of the dispersed fringes mode features.

Grating ($g\ mm^{-1}$)	Spectral width of images (nm)	
	Blue camera	Red camera
1800	2.75	6.7
300	16	40
100	50	120

Table 2. Features of the ten narrow and six wide bandwidths for the blue multi-chromatic mode calculated at 570 nm.

Grating ($g\ mm^{-1}$)	Spectral width of images (nm)	
1800	$\Delta\lambda_n = 0.05$	$\Delta\lambda_w = 0.25$
300	$\Delta\lambda_n = 0.3$	$\Delta\lambda_w = 1.5$

Table 3. Features of the four bandwidths for the red multi-chromatic mode calculated at 700 nm.

Grating ($g\ mm^{-1}$)	Spectral width of images (nm)		
1800	$\Delta\lambda_1 = 0.6$	$\Delta\lambda_2 = \Delta\lambda_3 = 0.3$	$\Delta\lambda_4 = 2$
300	$\Delta\lambda_1 = 4$	$\Delta\lambda_2 = \Delta\lambda_3 = 2$	$\Delta\lambda_4 = 12$

In section 2 we describe the strategy of dispersion correction adopted for the GI2T-REGAIN spectro-interferometer. Section 3 deals with numerical results for glass thickness and visibility. In section 4 we describe the optical system designed to compensate for the dispersion within our instrument.

2. The theoretical concept of GI2T-REGAIN dispersion compensation

2.1. The GI2T-REGAIN spectro-interferometer

The full description of the GI2T-REGAIN interferometer was given by [10, 11]. The GI2T-REGAIN interferometer is composed of two 1.5 m afocal telescopes with image plane recombination. Its north–south baseline can vary from 12 to 65 m. The REGAIN spectrograph is implemented at the visible focus. It has two photon-counting cameras which work in parallel on separate spectral regions centred at 570 and 700 nm. Three different gratings (R_1 : 1800 $g\ mm^{-1}$, R_2 : 300 $g\ mm^{-1}$, R_3 : 100 $g\ mm^{-1}$) provide a wide range of spectral resolutions reaching the value of 30 000. The spectrograph can work in two different modes selected by the entrance focal plane optics: the dispersed fringes mode and the multi-chromatic mode. Tables 1–3 summarize the spectral features of images recorded at the interferometric focus. In the dispersed fringe mode each detector records a single dispersed image. In the multi-chromatic mode, several filtered adjacent images are formed in each camera. There are four images within the red camera and 16 within the blue camera.

2.2. Specific requirements

Several authors have described methods for dispersion compensation. The analysis of [16] attempts to ensure that the OPD of two narrow and widely separated spectral bands are identical. The authors of reference [6] developed a method which determines the appropriate glass thickness from the optical path equalization at two different wavelengths. References [3, 7, 8, 15] focused on equations that constrain the derivatives of the fringe phases. However, they are not adapted to the specific requirements of the GI2T-REGAIN interferometer, because they aim to minimize the OPD without maximizing the fringe contrast. We keep, as in the previous methods, the principle of visibility maximization. Nevertheless, we do not consider phase derivatives and we perform calculations for several bandwidths. These bandwidths are either contiguous for what concerns the images of the same multi-chromatic mode or separated if we consider images from the two different cameras.

The dispersion compensating systems (DCS) have to operate in any of the spectrograph configurations described in section 2.1. We thus had to develop a control system which provides enough flexibility to integrate the corresponding features:

(i) The blue or the red camera used in the multi-chromatic or dispersed fringes modes.
(ii) Two cameras working in both the multi-chromatic or dispersed fringes modes. We can either optimize the compensation for one camera, or for both, simultaneously.

In the first case the correction achieved within the reference camera is of better quality. In the second case the correction level is nearly the same in both cameras.

The delay line operation has to be coordinated with the DCSs to allow accurate correction of the dispersion and high-quality fringe tracking. In the new configuration of GI2T two fringe trackers are available. RAFT (Rapid Active Fringe Tracker) operates in the dispersed fringe mode. This tracking system has been described by [5]. Efficient coherencing is ensured provided that the signal-to-noise ratio (SNR) in the Fourier transform of the dispersed image is high enough. The result of the dispersion compensation is an improvement on the performance of RAFT. It will enable fringe tracking with a fainter source and with lower visibilities. Nevertheless the use of a slit still limits the achievable limiting magnitude. This problem will be solved by implementing a new fringe tracker operating in the multi-chromatic mode [11]: SIFT (Spectro-Imaging Fringe Tracker). Multi-chromatic imaging modes were known to be useless in ground-based interferometry because of the poor fringe contrast resulting from atmospheric dispersion, unless used with narrow spectral bandwidths, thus drastically limiting their field of application. The implementation of DCSs restores the fringe contrast and enables the use of multi-chromatic fringe tracking.

In parallel to the visible spectrograph, dedicated infrared (IR) instruments have been developed to achieve IR interferometric measurements at the REGAIN IR focus [12, 18]. Simultaneous IR and visible observations are achievable. Nevertheless, this observation mode requires special care in the use of dispersion compensation for the visible region. Indeed dispersion correction is not required in the IR region. Thus the glass thicknesses calculated for the visible region may corrupt the IR fringes depending on the context of observation. Whereas the glass thickness straightens the visible fringes, it curves and tilts the IR ones. Nevertheless, visible and IR fringes can be used simultaneously to achieve wavelength boot-strapping, thus enabling low-contrast visible fringes to be recorded by tracking fringes in the IR region. We can also perform simultaneous visible and IR measurements very well in cases where no correction is required. This mainly concerns cases that involve targets with small zenithal angles, short baseline or narrow bandwidth measurements.

2.3. Chosen criterion

A suitable criterion used for the selection of the appropriate glass thickness is the visibility of the central fringe. The optimum thickness gives the visibility a maximum value over the whole image bandwidth. The dispersion effect to be corrected depends on the difference between the vacuum OPD and the optical path introduced to balance it. The larger the difference, the larger the fringes contrast degradation. The procedure adopted to carry out the correction thus depends on different parameters: the first one is the difference between the refractive indices of air and vacuum. Due to the air index chromatism, the effect increases with shorter wavelengths λ. This also depends on the local atmospheric pressure P and temperature T. The second parameter is the baseline projected on the line of sight. Larger projected baselines yield a greater effect.

For a point source, the squared visibility function for the central fringe is given by [13]

$$V^2 = \left| \frac{\int_0^{+\infty} I(\sigma)\exp(-\mathrm{i}2\pi\sigma\delta(\sigma))\,\mathrm{d}\sigma}{\int_0^{+\infty} I(\sigma)\,\mathrm{d}\sigma} \right|^2 \tag{1}$$

where the wavenumber $\sigma = \frac{1}{\lambda}$ has been used instead of the wavelength λ and $\delta(\sigma)$ is the overall OPD. The spectral density distribution $I(\sigma)$ is supposed to be flat over the range $\Delta\sigma$ and equal to zero elsewhere. We then expand the exponential function in a Taylor series about the quantity $\mp\mathrm{i}2\pi\sigma\delta(\sigma)$ up to the second order. After some rearrangement, in the case of small visibility losses, equation (1) can be written as

$$V^2 \sim 1 - 4\pi^2\left(\frac{1}{\Delta\sigma}\int_{\Delta\sigma}(\sigma\delta(\sigma))^2\,\mathrm{d}\sigma - \left(\frac{1}{\Delta\sigma}\int_{\Delta\sigma}\sigma\delta(\sigma)\,\mathrm{d}\sigma\right)^2\right) \tag{2}$$

where the second term is proportional to the variance $\mathcal{V}[\sigma\delta(\sigma)]$:

$$\mathcal{V}[\sigma\delta(\sigma)] = \frac{1}{\Delta\sigma}\int_{\Delta\sigma}(\sigma\delta(\sigma))^2\,\mathrm{d}\sigma - \left(\frac{1}{\Delta\sigma}\int_{\Delta\sigma}\sigma\delta(\sigma)\,\mathrm{d}\sigma\right)^2. \tag{3}$$

This variance has to be minimized to obtain the maximum central fringe visibility. This can be easily understood since this variance describes the mean square deviation of the fringe phase values referred to the centroid calculated over the whole bandwidth. One can write the OPD at a given wavenumber between the two interferometric beams as

$$\delta(\sigma) = B\sin(z_\mathrm{p}) + n_\mathrm{air}(\sigma)\cdot x + t_\mathrm{glass}\cdot(n_\mathrm{air}(\sigma) - n_\mathrm{glass}(\sigma)) \tag{4}$$

where x depends on the positions of the telescopes and the delay line. The change in the projected zenithal angle z_p introduced by the atmosphere has been neglected. Here t_glass is the difference in glass thickness between the two DCSs. The quantities n_air and n_glass are the refractive indices of air and glass, respectively. We have chosen to use the equation for the refractive index of air n_air taken from astrophysical quantities [1]:

$$(n_\mathrm{air}^{P,T}(\sigma) - 1)\times 10^6 = \left(64.328 + \frac{29\,498.1}{146-\sigma^2} + \frac{255.4}{41-\sigma^2}\right) \times \left(\frac{P(1+(1.049-0.0157T)\times P\times 10^{-6})}{720.883(1+0.003\,661T)}\right) \tag{5}$$

where P is in mmHg, T in °C and σ given in $\mu\mathrm{m}^{-1}$. Throughout we have assumed $T = 7$ °C and $P = 875$ mbar which are averaged measured values at our site. The free parameters for the fringes visibility maximization are x and t_glass. A given configuration (λ, $\Delta\lambda$, P, T, B, z) yields the corresponding (x, t_glass) which maximize the fringe contrast. We considered x as a free parameter because the maximum fringe contrast can occur at a non-zero OPD.

The obtained glass thickness depends on the type of glass used for the compensation. The chosen material is Corning glass BSC B16-64 (equivalent to BK7) whose glass index is given by

$$n_\mathrm{glass}^2 = a_0 + \frac{a_1}{\sigma^2} + a_2\sigma^2 + a_3\sigma^4 + a_4\sigma^6 + a_5\sigma^8 \tag{6}$$

where the value of the a_i coefficients are shown in table 4.

Table 4. BSC B16-64 dispersion formula constants.

Coefficient	Value
a_0	$+0.227\,1176\times 10^{+6}$
a_1	$0.979\,9709\times 10^{-2}$
a_2	$+0.110\,9710\times 10^{-1}$
a_3	$+0.462\,2809\times 10^{-4}$
a_4	$+0.161\,6105\times 10^{-4}$
a_5	$-0.828\,5504\times 10^{-6}$

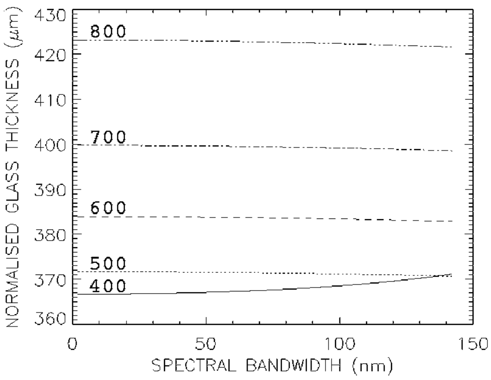

Figure 1. The plot shows the optimal glass thickness normalized to $B\sin(z_\mathrm{p})$. The variations versus wavelength and bandwidth are fixed by the type of glass used for the correctors.

This material is well suited for such an application when one considers its refractive indices (about 1.5) and its good transmission. The transmission for a 10 mm glass thickness varies from 0.997 at 400 nm to ≈0.9 at 2.2 μm.

3. Numerical results

If atmospheric dispersion is not compensated for, the 1% maximum tolerance, fixed for the visibility losses, limits the

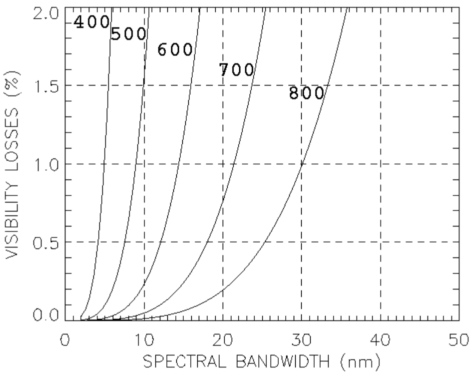

Figure 2. Computed visibility losses for a baseline of 50 m and a zenith angle of 30° without dispersion correction. The plot is given versus bandwidth for different central wavelengths.

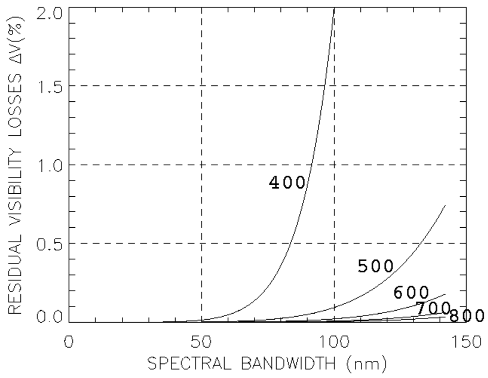

Figure 3. Residual visibility losses for a baseline of 50 m and a projected zenith angle of 30° with dispersion correction. The plot is given versus the bandwidth for different central wavelengths.

maximal spectral bandwidth over which visibility is calculated to values well above the limit fixed by the spectral decorrelation ∼50 nm and the spectrograph features. Compensation has to be carried out to override this limitation according to the chosen configuration for the REGAIN spectrograph.

If observations are performed using any of the two cameras in the dispersed fringe mode the correction for the dispersive effect is required. Nevertheless, when working with the most dispersive grating, the effect becomes negligible for wavelengths greater than 450 nm. Compensation is unnecessary if measurements are performed in the blue multi-chromatic mode because of the small bandwidths involved. Figure 2 shows that for any bandwidth displayed in table 2, the visibility losses are less than 0.1%. With respect to the red multi-chromatic mode, a correction is required with the 300 g mm^{-1} grating. In this mode, four spectrally filtered images in adjacent spectral bands are recorded. The correction to be applied is computed from the larger bandwidth features. We also had to consider the case where the two output cameras are used simultaneously. Due to the grating dispersion this configuration cannot be put into operation with the 100 g mm^{-1} one. The optimal glass thickness is now deduced from the minimization of a combined variance $\mathcal{V}$, where $\mathcal{V}$ is given by the sum of the variance calculated for each camera.

It is of interest to calculate the expected gain in visibility in both modulus and phase. Figure 3 shows that the theoretical residuals on visibility are very low for the spectral bandwidth which do not exceed the spectral decorrelation limit (∼50 nm). The spectral decorrelation effect is now the limiting factor regarding the bandwidth over which the visibility is calculated. The optimal glass thickness not only yields an improvement in the fringes contrast but also stabilizes their phase. Figure 4 shows that the phase can be stabilized within 8° over a 100 nm bandwidth for the less dispersive mode. Within the more dispersive modes the phase variations over the whole bandwidth are well above 1°. Thanks to that we will be able to improve the quality of differential phase measurements. The accuracy achievable with the previous GI2T recombination was about 5° [17]. This feature is very interesting since differential interferometry provides measurements of stellar structure positions with sub-milliarcsecond resolution.

We even show that for the first time, we will be able to produce usable images in the multi-chromatic mode. Since

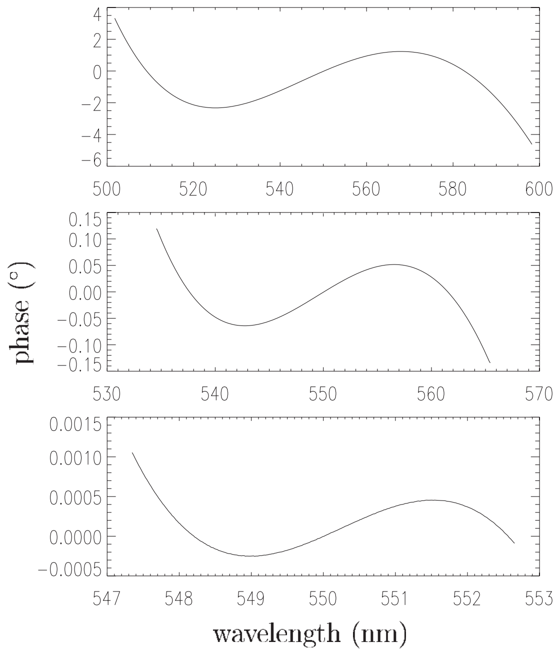

Figure 4. Phase variations versus wavelength for the three REGAIN gratings. From the less dispersive to the most dispersive one, from top to bottom.

this mode uses full-size speckled images, it has a better SNR compared to the dispersed fringe mode. We will be able to reach fainter magnitudes and achieve low-visibility measurements without altering data accuracy. The gain in the SNR is increased by about a factor of five between images recorded in the multi-chromatic mode and images recorded in the dispersed fringes mode as shown in table 5.

4. The compensating systems optical design

Different spectrograph configurations as well as several baselines can operate during the same night at the GI2T-REGAIN interferometer. The atmospheric dispersion features can thus be extremely variable. The DCSs have been designed to provide an equivalent flexibility in their operation. We first aimed to having a continuously variable glass thickness in order to fit the calculated optimum thickness. We then

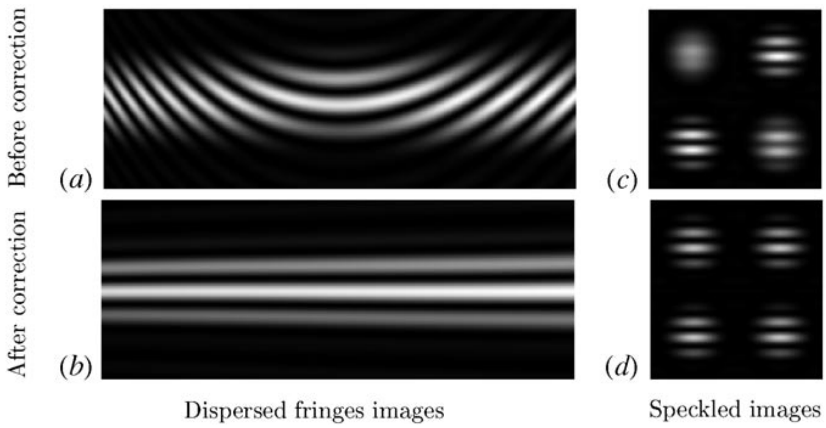

Figure 5. Predicted fringe patterns for a baseline of 50 m and a zenith angle of 30°. Raw images degraded by the atmospheric dispersion effect (top panels). Images obtained by introducing the correction of the DCSs and fringe trackers (bottom panels). The dispersed fringes images are computed for a 100 nm bandwidth centred on 550 nm (*a*) and (*b*). Fringes at different wavelengths are shifted with respect to each other. The fringe system appears curved (*a*). The dispersion correction cancels this chromatic effect (*b*). The multi-chromatic images (*c*) and (*d*) show the effect of dispersion when the 100 g mm^{-1} grating with the larger bandwidth image centred on 650 nm is used. Without any correction, the fringes contrast in the wide spectral channel image is very low (*c*), whereas DCSs yield usable images (*d*).

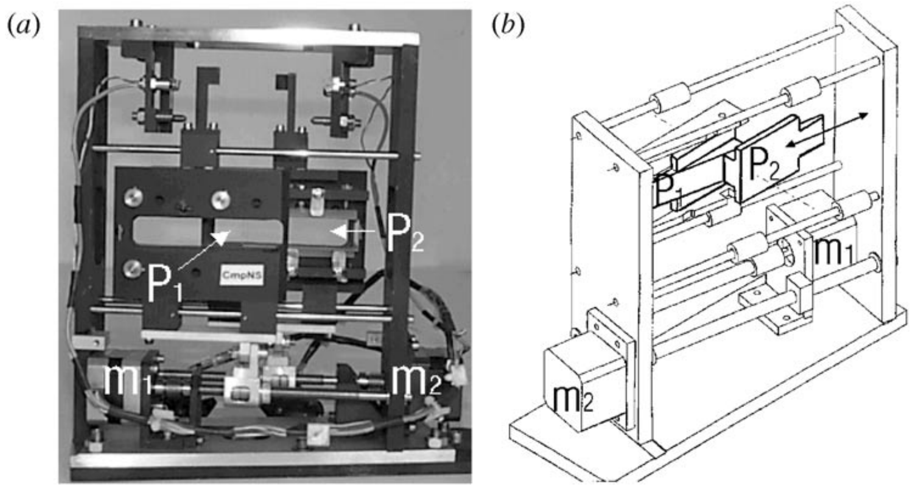

Figure 6. (*a*) A photograph of one of the DCSs showing the two prisms P_1, P_2 embedded in their translating mounts. (*b*) Schematic to focus on the prisms implementation in the modules. Stepping motors m_1, m_2 move the prisms along their hypotenuse faces. The prisms set can then be compared to a glass plate with continuously variable thickness.

Table 5. Comparison of the expected SNR achieved using the dispersed fringes mode or multi-chromatic mode.

	(a)	(b)
r_0 (cm)	7	7
Visibility (%)	100	10
Stellar magnitude	6	2
Spectral bandwidth (nm)	12	12
Integration time (s)	180	180
SNR x–λ mode	5.3	2.1
SNR multi-chromatic mode	25.3	10.4

wanted to have the option of observing without any dispersion correction. Such constraints ruled out designs based on plate sets added to one or the other beam which change the glass path by a fixed amount. The final design, shown in figure 6, comprises of two prisms with facing hypotenuse sides.

Our stepping motors provide 200 full steps per revolution and allow operation in half-step mode. They have a 2.5 μm prism-positioning resolution in half-step mode. This yields a 0.5 μm glass thickness resolution. This value is well above the requirements derived from the maximum acceptable visibility loss. The calibration of the glass thickness versus the motor step law has been carried out using the combination of two measurement sets:

- We have derived measurements of the glass thickness variation with respect to the minimum thickness (a function of the prisms positions) using a laser metrological system. This system records the change in OPD produced by the glass thickness variation with a 1 μm accuracy.
- We have carried out a few absolute measurements of the glass thickness using a laboratory-based Michelson interferometer. In this experiment we have compared the glass thickness introduced with one DCS to a reference glass plate of the same material.

From these measurements, we achieve a 20 μm accuracy in the glass thickness control. A 20 μm error in the introduced glass thickness does not affect the fringe contrast or the visibility phase. Indeed the mean OPD due to that error is compensated for by the active fringe tracking system.

5. Conclusion

In this paper we have presented the atmospheric DCS used within the GI2T-REGAIN long baseline stellar interferometer. These systems have been designed to provide an efficient correction in both the dispersed fringe mode and the multi-chromatic mode of the REGAIN spectrograph. The dispersive properties of variable glass thickness are used to compensate for the atmospheric dispersion effect caused by the use of an air-filled delay line.

The implementation of DCSs permit us to estimate the visibility at larger bandwidths since the corrected dispersed interferograms are no longer curved. We can thus achieve a higher SNR in the dispersed fringe mode if the atmospheric dispersion effect is compensated for. We have also shown that the quality of differential phase measurements is enhanced since the relative fringes phase is stabilized by the correction achieved. Consequently, sub-milliarcsecond astrometric measurements of stellar structures can be achieved. This would be particularly interesting for studying the morphology and circumstellar environment of interacting Be binary stars such as β Lyrae or ϕ Persei. Moreover, the use of DCSs permit us to access a larger hour angle range ($\pm 3h$). We will then benefit more from the earth-rotation synthesis effect.

Thanks to the implementation of these compensating systems, for the first time the GI2T-REGAIN stellar interferometer will produce usable large spectral band images in the multi-chromatic mode. This will allow a significant improvement of the SNR compared to the dispersed fringe mode. Since GI2T is a multi-speckle interferometer, the use of full-sized filtered images can efficiently exploit the recorded intensity and consequently achieve higher limit magnitudes until the adaptive optics systems currently under development at GI2T will be implemented.

Acknowledgments

I would like to thank Sylvestre Rebattu, Guy Merlin and Alain Spang who ensured the technical support to achieve the calibration and implementation of the DCSs and their control system. I thank Denis Mourard and Daniel Bonneau for their useful criticism.

References

[1] Allen C W 1973 *Astrophysical Quantities* (London: Athlone)
[2] Davis J, Tango W J, Booth A J, ten Brummelaar T A, Minard R A and Owens S 1999 *Month. Not. R. Astron. Soc.* **303** 773
[3] Davis J , Tango W and Thorvaldson E D 1998 *Appl. Opt.* **37** 5132
[4] Haniff C A, Baldwin J E, Boysen R C, George A V, Buscher D F, Mackay C D, Pearson D, Rogers J, Warner P J, Wilson D M A and Young J S 2000 *SPIE Proc.* **4006** 627
[5] Koechlin L, Lawson P R, Mourard D, Blazit A, Bonneau D, Morand F, Stee Ph, Tallon-Bosc I and Vakili F 1996 *Appl. Opt.* **35** 3002
[6] Lacasse M G and Traub W A 1988 *High-Resolution Imaging by Interferometry* p 959
[7] Lawson P R 1996 *Appl. Opt.* **35** 5122
[8] Lawson P R and Davis J 1996 *Appl. Opt.* **35** 612
[9] Lévèque S, Koehler B and von der Luhe O 1996 *Astrophys. Space Sci.* **239** 305
[10] Mourard D *et al* 2000 *SPIE Proc.* **4006** 434
[11] Mourard D, Clausse J-M, Pedretti E, Pierron M, Dalla R, Dugué M, Koechlin L, Merlin G and Thureau N 2000 *SPIE Proc.* **4006** 541
[12] Rousselet-Perraut K, Haguenauer P, Petmezakis P, Berger J-Ph, Mourard D, Ragland S, Huss G and Reynaud F 2000 *SPIE Proc.* **4006** 1042
[13] Steward E G 1989 *Fourier Optics* (Chichester: Ellis Horwood)
[14] Tallon-Bosc I 1989 *PhD Thesis*
[15] Tango W J 1990 *Appl. Opt.* **29** 516
[16] ten Brummelaar T A 1995 *Appl. Opt.* **34** 2214
[17] Vakili F, Mourard D, Bonneau D, Morand F and Stee Ph 1997 *Astron. Astrophys.* **323** 183
[18] Weigelt G *et al* 2000 *SPIE Proc.* **4006** 617